ภาคผนวก ข
วารสารปริทรรศน์

Available online at www.sciencedirect.com
SCIENCE DIRECT®
Polymer Testing 25 (2006) 568–577
POLYMER TESTING
www.elsevier.com/locate/polytest

Product Performance

Final product testing of rotational moulded natural fibre-reinforced polyethylene

F.G. Torres*, C.L. Aragon

Polymers and Composites Group—POLYCOM, Catholic University of Peru, Lima 32, Peru

Received 8 February 2006; accepted 24 March 2006

Abstract

The process of rotational moulding of natural fibre-reinforced polymers (NFRPs) has been developed recently at POLYCOM. This process allows for the use of discrete natural fibres as an efficient reinforcing agent for thermoplastic matrices. In this way, hollow objects with acceptable properties can be produced. The results from different experimental tests carried out on samples taken from rotomoulded cylinders are presented in this paper. Mechanical tests, such as tensile, compression, impact, deep drawing and recovery were performed in order to characterise unreinforced and reinforced natural fibre samples. Other properties, such as environmental stress cracking resistance (ESCR) and shrinkage were also assessed. The results obtained indicate that, in most cases, the properties of natural fibre-reinforced composites are superior to those of the unreinforced ones. In some cases, however, lower mechanical properties have been reported for the reinforced specimens. The testing methodology described here can be used to assess the properties of both reinforced and unreinforced rotomoulded products.

Keywords: Natural fibres; Reinforcement; Rotational moulding; Mechanical properties; Physical properties

1. Introduction

Rotational moulding is a technique used mainly for the manufacture of hollow plastic parts. Typical rotational moulding products are toys, balls and storage tanks. More recently, the rotational moulding of high-density polyethylene has gained considerable importance, due to its proven advantages in the manufacture of hollow plastic products.

There have been only a few technological developments in rotational moulding and the knowledge of the process has essentially been based on trial and error. Not many studies have been carried out to understand the underlying principles that govern this process [1–8]. In that sense, powder processing of metals and ceramics has been the subject of more detailed studies and several models have been proposed to explain the different types of sintering processes that occur in industrial operations. In the polymer field, however, there is still discussion whether sintering or coalescence is the governing processes in the rotomoulding technique. Moreover, no consistent models have been produced to explain the processes of multicomponent or multiphase sintering with polymers.

*Corresponding author. Department of Mechanical Engineering, Pontificia Universidad Catolica del Peru, Av. Universitaria Cdra. 18, s/n, Lima 32, Peru.
E-mail address: fgtorres@pucp.edu.pe (F.G. Torres).

0142-9418/$ - see front matter © 2006 Elsevier Ltd. All rights reserved.
doi:10.1016/j.polymertesting.2006.03.010

In order to understand the sintering process, Gao and Mackley [8] and later Wu et al. [9] studied the different stages that occur during sintering of UHMWPE. Two main stages have been differentiated in the process. The first stage consists of the "accommodation" of the irregular particles under pressure and above the melting temperature, so that all large voids are removed. The second stage consists of the self diffusion over the whole molecular length—and not just over the length of chain-ends [9]. The sintering behaviour and the bubble formation process in rotomoulding have also been studied by Crawford et al. [10,11].

The work presented in this paper is part of a long-term research project started at POLYCOM-PUCP that studies natural fibre-reinforced polymers (NFRPs) [12–19]. It studies the characterisation of natural fibre-reinforced and unreinforced polymer samples produced with the rotomoulding technique.

Natural plant fibres have been used in the past as a reinforcing material for different types of matrices [20–23]. In recent years, attention has been paid to their use as a reinforcing material for thermoplastics. In particular, the automotive industries have shown interest in the advantages that this type of fibre-reinforced system can provide [20,21]. The advantages of biofibres over traditional fibre reinforcements, such as glass fibres, are: low cost, low density (good specific properties), reduced wear in processing equipment, high toughness, biodegradability and "ecological friendliness" (since they can be produced from renewable resources).

2. Description of the NFRTP rotomoulding process

In a previous paper we introduced the rotomoulding process for NFRP systems [12,13]. Briefly, a cylindrical two-part stainless-steel mould is loaded with polymer powder or polymer and fibre together. Then the mould is rotated in two axes at relatively low speeds (usually 10–30 rpm in industrial operations) while being heated, so that particle consolidation can take part. Then the mould is cooled down and the product is extracted from it. Before loading the polymer or polymer composite, a demoulding agent is applied to the internal surface of the mould.

Heating was achieved in a chamber fitted with heat-resistant glass panels, by means of a Leister hot air blower. Rotation in the first axis was achieved with an electric DC motor, so that speed could vary over the processing range. Rotation in the second axis was achieved by means of a light weight gear box that transmitted the movement from the first axis with a controlled transmission rate. The rotating speed in the first axis was registered with a tachometer.

3. Experimental

3.1. Materials

Rotomoulded cylinders were made of HDPE powder with an MFI 2.8 (190 °C/2.16 kg). Powder morphology was non-spherical. Cabuya (*Furcraea Cabuya*) and sisal (*Agave Sisalana*) fibres with an average length of about 5 mm were added as reinforcement at concentrations varying from 0% to 7.5% by weight.

3.2. Sample preparation

Previous to the experiments, the fibres were treated with non-ionic soap at a concentration of 3% v/v at 65 °C for 1 h with constant agitation. The soap was then washed out with water and the fibres were left for 24 h in an oven at 65 °C. Next, they were treated with 0.3 g of stearic acid dissolved in 9 ml of acetone for every 10 g of fibre used [19]. After the acetone had evaporated, fibres were dried again for 24 h at 70 °C. Silicone was used as a demoulding agent. The composite cylinders were prepared as follows: A first load consisting of the first layer of HDPE and all reinforcing fibres was rotomoulded for 10 min at 170 °C. After the process was completed, a second load of pure HDPE was added to the mould. This second load was rotomoulded for 10 min at 170 °C. The mould was cooled down with a fan for 10 min. At this stage, the cylinder could be demoulded.

Double-layer cylinders were produced when reinforcing fibres were used. Single-layer cylinders were produced, when only pure HDPE was used.

Table 1 presents the loads of material used in the rotomoulding process.

3.3. Testing methods

Mechanical and physical tests were carried out with the specimens processed at different conditions. The mechanical tests considered were: tensile strength, impact, compression, indentation and recovery. Other physical properties such as shrinkage, environmental stress cracking resis-

Table 1
Material loads used in the preparation of the rotomoulded specimens

	Fibre dosification			
	0%	2.5%	5.0%	7.5%
Fibre (g) (only first load)	0	1.5	3	4.5
HDPE: first load (g)	60	20	20	20
Total first load (g)	60	21.5	23	24.5
Second load (g) (HDPE only)	0	38.5	37	35.5
Total load (g)	60	60	60	60

tance (ESCR), thickness and density were also performed.

One of the advantages of the rotomoulding process for NFRTPs is that an almost isotropic coherent fibre mat is formed. In previous works we have found that for specimens prepared using this technique, the effect of anisotropy on mechanical properties was not too significant [13,18]. For that reason, in the present work all specimens have been taken from the same direction.

3.3.1. Tensile strength

The samples used for the tests are shown in Fig. 1. The specimen dimensions were: $a = 20 \times 10^{-3}$ m, $b = 60 \times 10^{-3}$ m and $c = 3 \times 10^{-3}$ m. They were obtained from the cylinder walls. The tests were carried out in a Hounsfield tensile tester at room conditions and at a speed of 3.82 mm/min. The ultimate tensile strength (UTS) was obtained from this test.

3.3.2. Impact

Impact strength tests [24] were carried out using a 65 J Hounsfield balanced impact machine. Unnotched specimens with dimensions $a = 13 \times 10^{-3}$ m, $b = 48 \times 10^{-3}$ m and $c = 3 \times 10^{-3}$ m (see Fig. 1), obtained from the cylinder walls, were used in this test. Fig. 2 shows the configuration used in the tests.

3.3.3. Compression

Compression tests were carried out in a universal testing machine manufactured by MLF. A rotomoulded cylinder was compressed in its axial direction, as shown in Fig. 3. Maximum load at compression and maximum compression load without plastic deformation were recorded in these experiments.

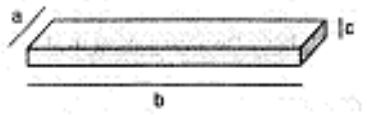

Fig. 1. Specimen geometry for tensile tests (strips were cut from the walls).

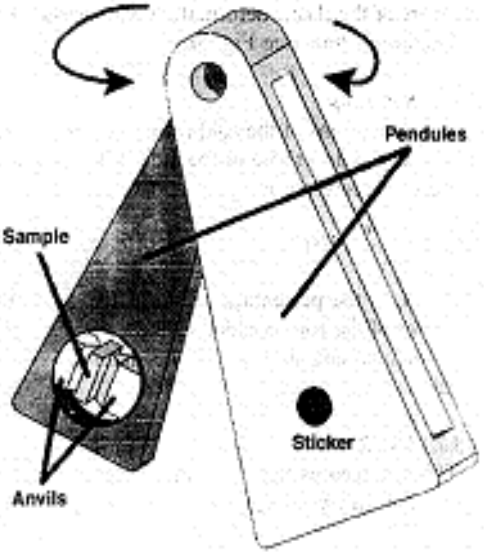

Fig. 2. Test disposition for impact tests.

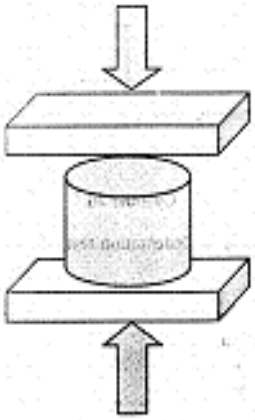

Fig. 3. Compression test scheme.

3.3.4. Indentation

Indentation tests were carried out using a "deep drawing machine" fitted with a (steel) sphere 19×10^{-3} m in diameter. The specimens were obtained from the lids of the rotomoulded cylinders. Maximal

indentation depth was measured before the specimen broke. Fig. 4 shows the arrangement used for this test.

3.3.5. Recovery

The recovery test measures the elastic recovery of a rotomoulded cylinder. The specimens were compressed by 20% in the same machine described in Section 3.3.3 at a speed of 3 mm/min. Then, the recovery of the elastic deformation was measured as a function of time (see Fig. 5).

3.3.6. Shrinkage

The dimensions of the cold rotomoulded cylinder were compared to those of the mould. Results were expressed according to

$$S_n = \frac{\phi_{rc} - \phi_m}{\phi_m} 100\%, \quad (1)$$

where S_n is the percentage of shrinkage, ϕ_{rc} is the diameter of the rotomoulded cylinder measured 1 h after demoulding and ϕ_m is the diameter of the mould.

3.3.7. ESCR

This test records the "premature" onset of crack formation and weakening of a polymeric component due to the simultaneous action of stress (or strain) and contact with a tensoactive agent. Samples from the cylinder walls of size $a = 13 \times 10^{-3}$ m and $b = 38 \times 10^{-3}$ m (see Fig. 1) were extracted; 10 samples were used for each test.

The samples were conditioned at laboratory temperature (23 °C) and atmospheric pressure for 40 h before the test actually begun. The samples were then notched to a depth of 0.5×10^{-3} m, bent through 180° and transferred to a metallic specimen holder [26]. The holders were introduced into test tubes filled with Nonyl-Phenol, a tensoactive substance, with a concentration of 10% v/v. The test tubes were closed and submerged in a heating bath at a temperature of 50 °C. Every 24 h, they were inspected to record any crack in their surface. The proportion of the total number of specimens that failed (presented cracks) was recorded as a function of time.

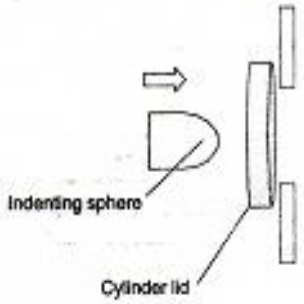

Fig. 4. Indentation test scheme.

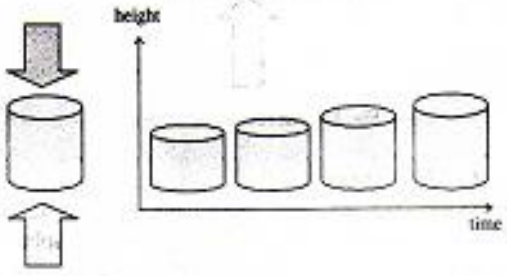

Fig. 5. Recovery test scheme.

3.3.8. Thickness

The thickness in different parts of the cylinder was measured using a vernier calliper. Three zones were considered for the readings: walls (10 measurements), upper lid (five measurements) and lower lid (five measurements).

3.3.9. Density

The displacement method was used in order to assess the density of the rotomoulded specimens [27]. A circular sample (20×10^{-3} m in diameter) was extracted from the walls of the rotomoulded cylinder. In order to avoid the absorption of water, the samples were completely covered with Teflon® film. Density was calculated, according to Eq. (2) [27]:

$$D = \frac{a}{(a+w)-b} 0.99756 \ (\mathrm{kg\,m^{-3}} \times 10^{-3}), \quad (2)$$

where a is the apparent mass of specimen, without wire or sinker, in air, b the apparent mass of specimen (and of sinker, if used) completely immersed and of the wire partially immersed in liquid and w the apparent mass of totally immersed sinker (if used) and of partially immersed wire.

4. Results and discussion

4.1. Tensile strength

As it can be seen in Fig. 6, sisal and cabuya fibres increase the UTS of the composite materials

compared to unreinforced HDPE. This tendency is in agreement with previous results reported for natural fibre-reinforced composites [16,20–23,25] and for long glass fibre composites [28,29]. In general terms, the increase in UTS is modest for both types of reinforcing fibres. As Fig. 6 shows, the best performance was obtained for cabuya fibres at a concentration of 2.5%, dropping sharply at 5%, even below that of unreinforced HDPE. On the other hand, sisal fibres decreased the performance of the material at a concentration of 2.5% but enhanced it at 5%.

Low mechanical properties at high fibre contents are mostly associated with the presence of fibre clumps and voids. Reinforcing discrete fibres increase the viscosity of the polymer matrix. This phenomenon has been reported for glass fibres [30] as well as for natural fibres [31]. An increased viscosity might also contribute to the formation of clumps during melt processing of natural fibre composites. With an adequate fibre treatment, this problem is reduced in the rotational moulding process of NFRTPs.

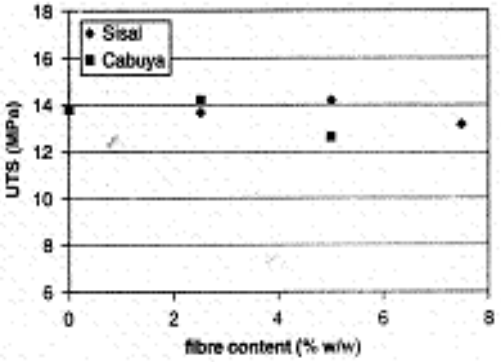

Fig. 6. Ultimate tensile strength (UTS) for reinforced and unreinforced specimens.

4.2. Impact

Fig. 7 presents the results for this test. As fibre content increases, the matrix becomes more brittle and the ability of the material to absorb impact energy decreases whatever the fibre used. Cabuya-reinforced HDPE absorbs more impact energy than sisal-reinforced HDPE at the same fibre content. A reduction of 55% in the ability to absorb energy is observed for sisal-reinforced HDPE at 7.5% fibre content relative to unreinforced HDPE. Fig. 8 shows an SEM photograph of a sample of 2.5% sisal-reinforced HDPE at the impact fracture zone. The two-layered structure already described in Section 3.2 (sample preparation) is visible here. In the unreinforced region, where bubbles are present, the morphology of a ductile fracture can be observed. On the other hand, the reinforcing fibres induce brittle fracture behaviour, as shown in Fig. 9. The same fracture patterns are shown in Fig. 10 for cabuya-reinforced HDPE.

4.3. Compression

A typical compression graph (stress vs. axial strain) showing the maximum compression load (the highest point in the curve) and the maximum elastic compression load is presented in Fig. 11. The maximum elastic compression load corresponds to

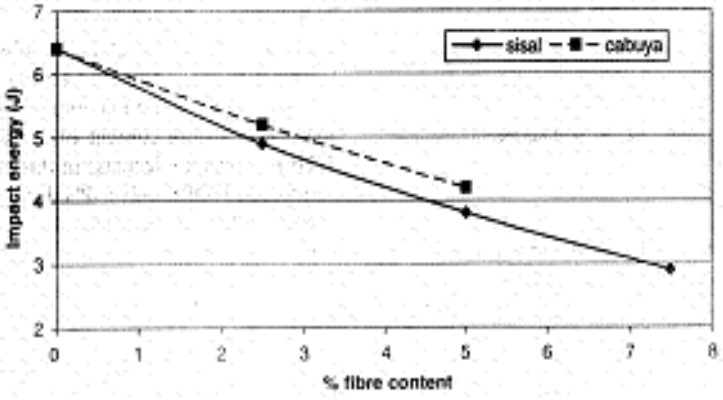

Fig. 7. Absorbed impact energy for reinforced and unreinforced specimens.

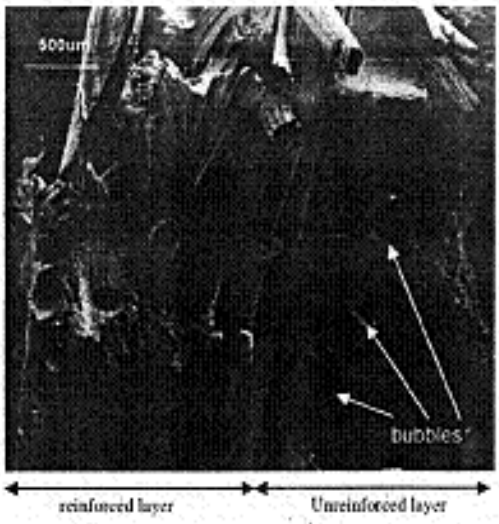

Fig. 8. SEM fractography for a sisal-reinforced specimen.

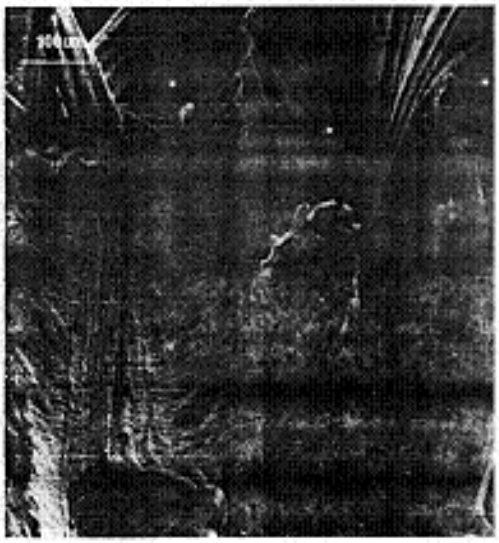

Fig. 9. SEM fractography for a sisal-reinforced specimen showing fibre fracture.

the point in the curve in which the increase in strain is no longer proportional to the increase in stress.

Fig. 12 gives the maximum compression load for sisal- and cabuya-reinforced HDPE. It can be observed (Fig. 12) that higher fibre contents correspond to lower compression loads for both types of reinforcing fibres.

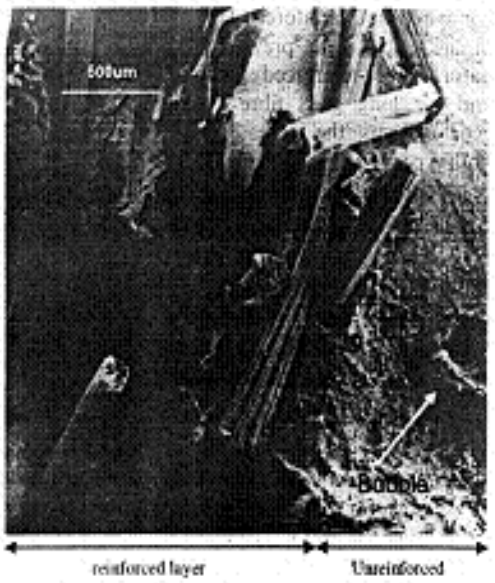

Fig. 10. SEM fractography for a cabuya-reinforced specimen.

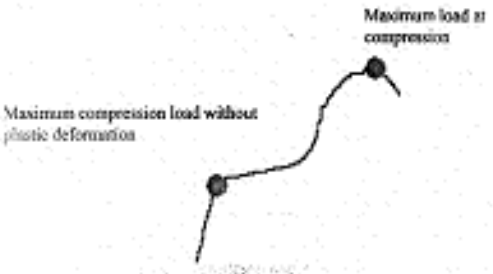

Fig. 11. Typical load vs. deformation graph obtained at compression tests.

Sisal-reinforced HDPE specimens have shown better performance in the compression mode compared to the cabuya-reinforced ones. This tendency was not found in tensile and impact tests.

Fig. 13 shows the maximum compression elastic load. For a fibre content of 2.5%, sisal-reinforced HDPE shows no decrease in this value and cabuya-reinforced HDPE only a 4% decrease with regard to the unreinforced specimens. In Fig. 14, the different tendencies in the stress–strain graphs can be observed for different fibre contents. By increasing fibre content, the yield zone can be found at lower loads. This means that fibres actually modify the mechanical properties of the polymer matrix by reducing the elastic region and inducing the formation of a longer plastic region.

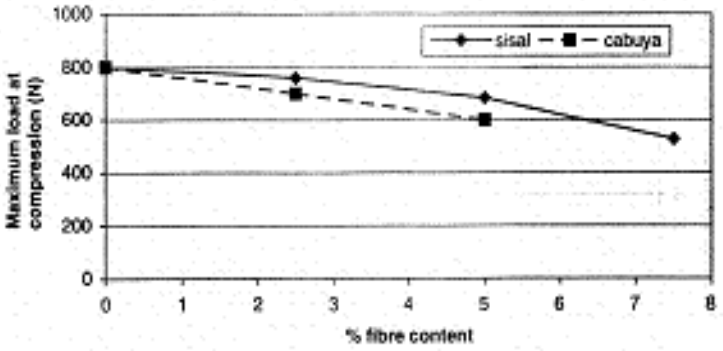

Fig. 12. Maximum loads at compression loads for reinforced and unreinforced specimens.

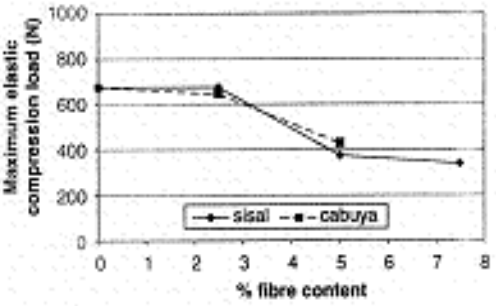

Fig. 13. Maximum elastic loads at compression loads for reinforced and unreinforced specimens.

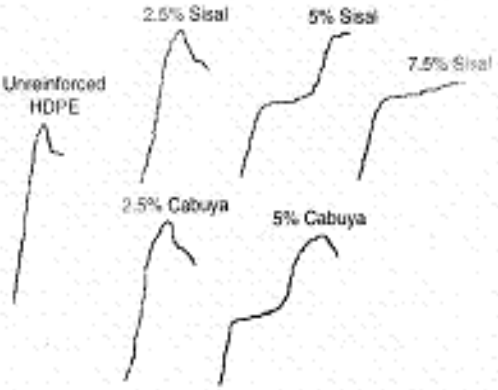

Fig. 14. Compression vs. deformation graphs obtained for different fibre types and contents.

4.4. Indentation

As shown in Fig. 15, sisal-reinforced HDPE specimens show greater indentation depths compared to the cabuya-reinforced ones. It is shown that by increasing fibre content, reinforced specimens tend to produce lower indentation depths. This indicates that the coherent fibre network increases the stiffness of the composite. The observed tendencies are in agreement with data from Fig. 12, which shows that sisal-reinforced specimens withstand higher compression loads at lower deformation levels.

4.5. Recovery

It can be observed (Fig. 16) that for most fibre contents, the rotomoulded cylinders recovered their original dimension after 1440 min, with cabuya-reinforced specimens showing the fastest response. However, for a fibre content of 7.5%, sisal-reinforced HDPE specimens showed a lower recovery response compared to the unreinforced ones. This might be due to possible fibre breakage during compression. In general, the fibre-reinforced specimens showed a more consistent elastic behaviour than the unreinforced ones. This might be due to the formation of a coherent fibre mat during the rotomoulding process. Fibre mat morphology for this process has been reported previously in the literature [13,18]. Dynamic mechanical analysis of long glass fibre-reinforced polypropylene sheets has shown that the formation of coherent mats enhances the elastic behaviour of the composite [29].

4.6. Shrinkage

Fig. 17 shows the percentage shrinkage, derived from Eq. (1), as a function of fibre content. It can be observed that with increasing fibre content the

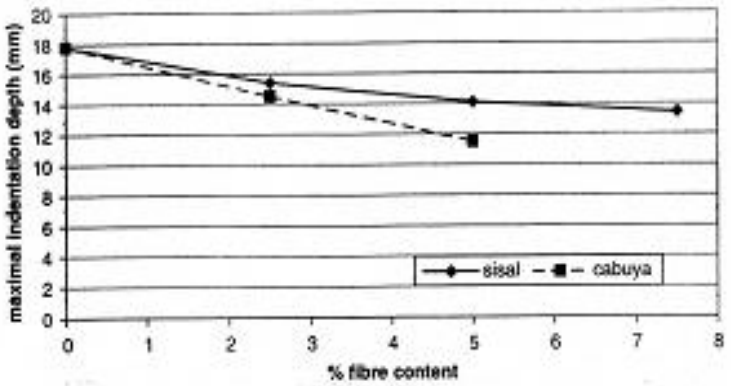

Fig. 15. Maximum indentation depth for reinforced and unreinforced specimens.

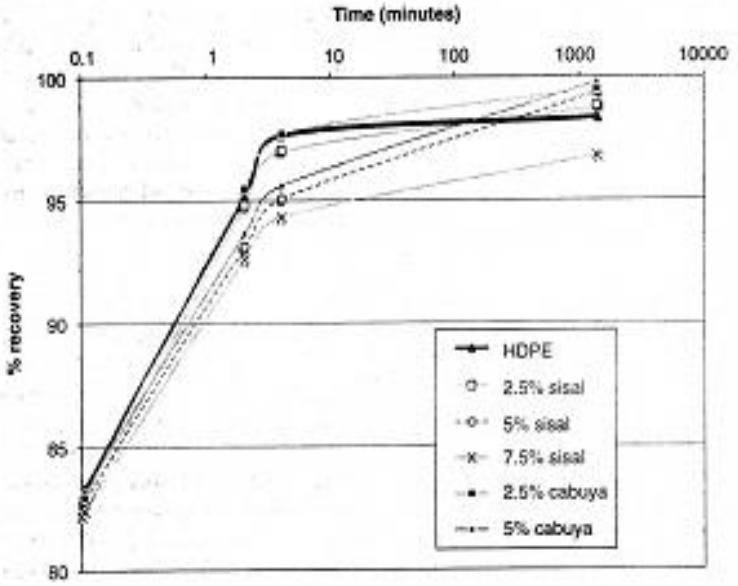

Fig. 16. Percentage of recovery measured for reinforced and unreinforced specimens.

percentage of shrinkage decreases, whatever the fibre used. However, there is a slight difference for a fibre content of 2.5%, where sisal-reinforced HDPE specimens showed less shrinkage than cabuya-reinforced ones.

4.7. ESCR

In Table 2, it can be observed that as fibre content increases, the rate of appearance of cracks rises for the first 48 h. This observation applied for both

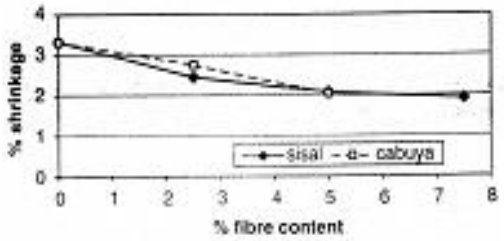

Fig. 17. Shrinkage measured for reinforced and unreinforced specimens.

types of fibres. No significant difference was observed between sisal- and cabuya-reinforced specimens.

4.8. Thickness

It can be observed from Table 3 that the lateral walls were always thinner than the lids (9% less compared to the mean value for unreinforced HDPE and between 4% and 8% for reinforced HDPE). For sisal- (5% and 7.5% w/w) and cabuya (2.5% and 5% w/w)-reinforced specimens, an increment in thickness with increasing fibre content can be observed.

4.9. Density

Fig. 18 presents the results from the density tests for sisal- and cabuya-reinforced HDPE specimens. It can be observed that density actually decreases with increasing fibre content, whatever the fibre used. This might be due to the fact that natural fibres act as a nucleating agent for bubbles and pores [32], accounting for the increase in porosity with sintering time.

Table 2
Results (number of cracks) from ESCR experiments

Time (h)	Number of cracks					
	HDPE	2.5% sisal	5% sisal	7.5% sisal	2.5% cabuya	5% cabuya
0	0	1	1	2	1	2
24	0	2	3	6	3	4
48	5	5	5	8	4	5
72	8	9	5	9	8	6
96	10	10	8	9	9	9
120			10	10	10	10

Table 3
Measured thickness at different positions of the rotomoulded specimens

	W (mm)	UL (mm)	LL (mm)	Mean (mm)
HDPE	2.93	3.29	3.47	3.23
2.5% sisal	2.95	3.25	3.41	3.2
5% sisal	3.15	3.36	3.73	3.41
7.5% sisal	3.49	3.64	3.91	3.68
2.5% cabuya	3.21	3.36	3.49	3.35
5% cabuya	3.44	3.64	3.84	3.64

W = walls; UL = upper lid; LL = lower lid.

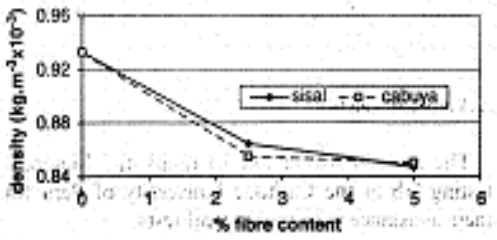

Fig. 18. Densities measured for reinforced and unreinforced specimens.

5. Conclusions

The mechanical properties of NFRPs processed by rotational moulding were characterised using several mechanical tests. Some relevant physical properties were also investigated.

The mechanical and physical properties of fibre-reinforced composites vary considerably with fibre content. Tensile strength results indicated that, depending on the fibre type, there is an optimal fibre content for which fibre-reinforced composites show the best properties. Beyond this optimal fibre content, tensile strength decreases due to the increased presence of bubbles and voids in the composites.

Impact behaviour was influenced by fibre type and content. Cabuya-reinforced composites showed higher impact strengths than the sisal-reinforced ones. In all cases, impact strength decreased with increasing fibre content.

Recovery tests showed that the coherent fibre mats formed during the rotomoulding process modify the elastic properties of the polymeric matrix. The resulting composite products show less plastic deformation and higher elasticity, accompanied by shorter recovery times.

Shrinkage tests showed that the shrinkage level of the natural fibre composites studied here decreases as fibre content increases.

At higher fibre contents, lower densities were obtained, mainly due to the formation of more voids and bubbles during the rotomoulding process. The testing methodology described here can be used to assess the properties of both reinforced and unreinforced rotomoulded products. A set of these tests may be suitable for mechanical testing of final rotomoulded products, or they could be combined

with specific physical testing such as ESCR, thickness measurement and density.

Acknowledgements

The authors would like to thank the Materials testing lab at the Catholic University of Peru for their assistance with mechanical tests.

References

[1] A. Siegmann, I. Raiter, M. Narkis, P. Eyerer, Effect of powder particle morphology on the sintering behaviour of polymers, J. Mater. Sci. 21 (4) (1986) 1180.
[2] N. Rosenzweig, M. Narkis, Sintering rheology of amorphous polymers, Polym. Eng. Sci. 21 (17) (1981) 1167.
[3] O. Pokluda, C.T. Bellehumeur, J. Vlachopoulos, Modification of Frenkel's model for sintering, AICHE J. 43 (12) (1997) 289.
[4] C.T. Bellehumeur, J. Vlachopoulos, Polymer sintering and its role in rotational molding, SPE ANTEC Tech Papers, 1998, p. 1112.
[5] M.A. Rao, J.L. Throne, Principles of rotational molding, Polym. Eng. Sci. 12 (4) (1972) 237.
[6] M. Kontopoulou, E. Takacs, C.T. Bellehumeur, J. Vlachopoulos, Resins for rotomolding: considering the options, Plastics Eng. 54 (2) (1998) 29.
[7] C.T. Bellehumeur, M. Kontopoulou, J. Vlachopoulos, The role of viscoelasticity in polymer sintering, Rheol. Acta 37 (1998) 270.
[8] P. Gao, M.R. Mackley, in: Proceedings of the Royal Society, Series A (Mathematical and Physical Sciences), London, vol. 444(1921), 1994, p. 267.
[9] J.J. Wu, C.P. Buckley, J.J. O'Connor, Processing of ultra-high molecular weight polyethylene: modelling the decay of fusion defects, Chem. Eng. Res. Des. 80 (A5) (2002) 423.
[10] R.J. Crawford, J.A. Scott, The formation and removal of gas bubbles in a rotational moulding grade of PE, Plast. Rub. Comp. Proc. Appl. 7 (1987) 85.
[11] R.J. Crawford, P.J. Nugent, A new process-control system for rotational molding, Plast. Rub. Comp. Proc. Appl. 17 (1) (1992) 23.
[12] F.G. Torres, M. Aguirre, G. Aguila, Paper presented at the Polymer Processing Society 18th Annual Meeting PPS-18, Guimarães, Portugal, 2002.
[13] F.G. Torres, M. Aguirre, Rotational moulding and powder processing of natural fibre reinforced thermoplastics, Int. Polym. Process. 18 (2) (2003) 204.
[14] F.G. Torres, M.L. Cubillas, Paper presented at the Polymer Processing Society 19th Annual Meeting PPS-19, Melbourne, Australia, 2003.
[15] F.G. Torres, M.L. Cubillas, J.F. Dienstmaier, Paper presented at the Polymer Processing Society 20th Annual Meeting PPS-20, Akron, OH, 2004.
[16] F.G. Torres, B. Ochoa, E. Machicao, Single screw extrusion of Natural Fibre Reinforced Thermoplastics (NFRTP), Int. Polym. Process 18 (1) (2003) 33.
[17] F.G. Torres, B. Ochoa, J. Nakamatsu, Paper presented at the Polymer Processing Society European Meeting, Antalya, Turkey, 2001.
[18] F.G. Torres, R.M. Diaz, Morphological characterisation of Natural Fibre Reinforced Thermoplastics (NFRTP) processed by extrusion, compression and rotational moulding, Polym. Polym. Comp. 12 (8) (2004) 705.
[19] C. Grande, F.G. Torres, Investigation of fibre organisation and degradation in single screw extrusion of natural fibre reinforced thermoplastics, Adv. Polym. Technol. 24 (2) (2005) 145.
[20] A.K. Mohanty, M. Misra, G. Hinrichsen, Biofibers, biodegradable polymers and biocomposites: an overview, Macromol. Mater. Eng. 276 (277) (2000) 1.
[21] D. Nabi Saheb, J.P. Jog, Natural fiber polymer composites: a review, Adv. Polym. Tech. 18 (4) (1999) 351.
[22] R.M. Rowell, A. Sanadi, D.F. Caulfield, R.E. Jacobson, in: A.L. Leão, F.X. Carvalho, E. Frollini (Eds.), Lignocellulosic Plastic Composites, USP & UNESP, São Paulo, 1997, pp. 23–51.
[23] A.K. Bledzki, S. Reihmane, J. Gassan, Thermoplastics reinforced with fillers: a literature review, Polymer-Plastics Tech. Eng. 37 (4) (1998) 451.
[24] BS 2728-3 Method 359B, 1999.
[25] R.B. Seymour, Reinforced Plastics Properties & Applications, ASM International, Materials Park, OH, 1991 (p. 257).
[26] ASTM D1693, 2001.
[27] ASTM D792, 2000.
[28] F.G. Torres, S.F. Bush, Sheet extrusion and thermoforming of long glass fibre (LGF) reinforced polypropylene, Composites A: Appl. Sci. Manuf. 31 (12) (2000) 1421.
[29] S.F. Bush, F.G. Torres, E.S. Erdogan, Study of the mechanical properties of discrete long glass fibre reinforced polymer sheets and their influence on the thermoforming process, in: Proceedings of the Seventh International Fibre Reinforced Components, 1998, FRC98, p. 237.
[30] S.F. Bush, F.G. Torres, J.M. Methven, Rheological characterisation of discrete long glass fibre (LGF) reinforced thermoplastics, Composites: Appl. Sci. Manuf. 31 (12) (2000) 1289.
[31] M.A. Lopez-Manchado, J. Biagiotti, M. Arroyo, J.M. Kenny, Ternary composites based on PP-EPDM blends reinforced with flax fibers. Part I: processing and thermal behaviour, Polym. Eng. Sci. 43 (5) (2003) 1018.
[32] F.G. Torres, M. Carrillo, M. Cubillas, Melt densification of polymeric powder beds filled with natural fibres, Polym. Polym. Comp., in press.